EARTHQUAKE ENGINEERING AND STRUCTURAL DYNAMICS
Earthquake Engng. Struct. Dyn. **28**, 841–855 (1999)

TWO-DIMENSIONAL SCATTERING OF SH WAVES DUE TO A DISCONTINUITY IN BEDROCK

ERNEST HEYMSFIELD*
Department of Civil and Environmental Engineering, Louisiana State University, 3510 CEBA Building, Baton Rouge, LA 70803, U.S.A.

SUMMARY

The direct boundary integral equation technique is applied to determine the impact on surface amplification caused by an inhomogeneity in a bedrock half-space. The particular soil-rock configuration studied is one in which a soil layer rests on a rock half-space which includes a rock inclusion. The particular rock inclusion considered for this study is a semi-infinite rock layer with its upper boundary bordering the soil layer. Materials are considered viscoelastic except for the section of the rock half-space below the level of the rock inclusion which is considered elastic. A parametric study is performed to determine controlling factors for surface displacement due to a vertically incident shear wave. The study includes varying the stiffness and the thickness of the inclusion for a range of frequencies. Solutions from a one-dimensional analysis are compared with the results of a two-dimensional analysis in order to establish limits inside of which a two-dimensional analysis is required. Copyright © 1999 John Wiley & Sons, Ltd.

KEY WORDS: soil amplification; seismic waves; rock discontinuity; boundary elements

1. INTRODUCTION

As seismic waves propagate through the earth's near-surface geology, earthquake motion can be greatly modified.[1] Exact solutions for the amplification of seismic waves are limited to the one-dimensional solution and two-dimensional solutions in the case of geometries in which separation of variables is applicable. The one-dimensional solution assumes that the seismic motion propagates through horizontal layers of homogeneous and isotopic material. A detailed discussion of the one-dimensional solution for anti-plane motion is included in References 2 and 3. The one-dimensional solution is commonly used, however a deficiency in the method is that it neglects the effect of any anomaly, whether in material or in topography. Still the one-dimensional analysis has been found to provide acceptable results at sites where the assumption of horizontal soil layers with constant material properties can be approximated. For other soil configurations, acceptable results from the one-dimensional analysis have been found for low-frequency waves. For high-frequency waves, scattering due to an anomaly is significant and therefore warrants a two-dimensional solution. Exact solutions for two-dimensional antiplane wave propagation problems are limited to geometries where separation of variables can be

* Correspondence to: Ernest Heymsfield, Department of Civil and Environmental Engineering, Louisiana State University, 3510 CEBA Building, Baton Rouge, LA 70803, U.S.A. E-mail: eheymsf@lsu.edu

CCC 0098–8847/99/080841–15$17·50

Received 27 January 1998
Revised 3 November 1998

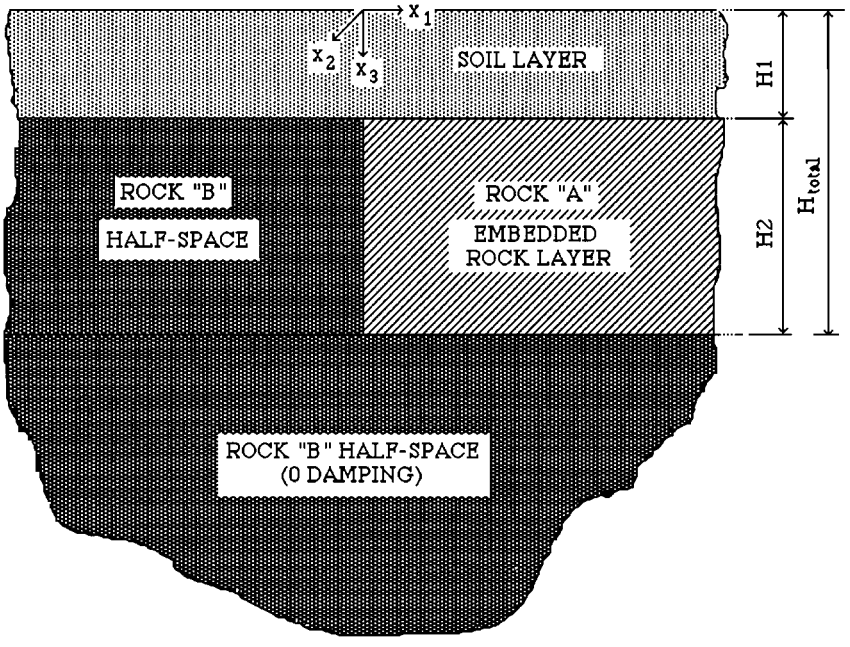

Figure 1. Soil-rock profile

applied and linear strain behaviour can be assumed. Various geometries possessing an analytic two-dimensional solution have been investigated. These analytic solutions include the amplification of an incident SH wave in a semi-cylindrical shape valley by Trifunac[4] and for a semi-elliptical alluvial valley by Wong and Trifunac.[5] Where analytic solutions are unavailable, numerical solutions must be resorted to. Different scenarios using numerical methods have been used. Dravinski[6] used the source method to investigate surface amplification for a soil profile consisting of dipping soil layers. This problem was also solved using wave functions by Eshraghi and Dravinski,[7] and the boundary element method by Dominguez and Abascal.[8] Vogt et al.[9] used the indirect boundary element method to investigate the influence that a canyon embedded in soil layers bounded by rock has on soil amplification. Hadley et al.[10] used the direct boundary element method to study cavities within half-spaces, surface irregularities, and inhomogeneities in soil layers for out-of-plane motion. Bouchon et al.[11] investigated amplification of SH wave motion for multi-layer soil configurations with non-horizontal interfaces. Bouchon and Coutant[12] examined this configuration for Love (Lg) waves. Prior work has focused on the effect that soil-layer geometry and soil properties have on the amplification of seismic motion. The intent of this paper is to investigate the effect that a bedrock discontinuity has on surface amplification and its significance when compared to the one-dimensional analysis solution.

The soil-bedrock configuration investigated is shown in Figure 1 with the soil and rock properties given in Table I. These properties represent typical values for sand and limestone rock. During seismic motions, non-linear stress–strain behaviour develops. In order to consider this non-linearity, an equivalent linear model is applied. In the model, an adjusted shear modulus and hysteretic damping is included to consider energy loss during the cyclic loading.[13] The values

Table I. Soil and rock properties

Soil properties		
Poisson's ratio (v_s)	0·25	
Damping (β_s)	5·00%	
Rock properties		
	Rock "A"	Rock "B"
Unit wt. ratio (γ_r/γ_s)	1·32	1·32
Poisson ratio (v_r)	0·25	0·25
Damping (β_r)	2·00%	1·00%
Shear wave vel. ratio C_s (rock)/C_s (soil)	Varies	10·00

given in Table I represent the adjusted shear moduli and hysteretic damping used in this analysis. These values remain constant during the analysis. The 0 damping for "Rock B" below H_{total} is necessary for the application of the half-space correction for this infinite domain. This is discussed later in the paper.

A parametric study is performed using a two-dimensional analysis. In the study, the amplification of vertically incident anti-plane shear waves is investigated as a function of embedded rock layer thickness and embedded rock layer shear velocity. The ratio of the embedded rock layer thickness to the soil layer thickness include: 1, 2, and 5. Three different shear velocity ratios of Rock "A" to the soil are studied: 1, 2·5, and 5. The shear velocity ratio of 1 is synonymous with the embedded material being soil and the rock half-space having a step. Results are determined as a function of a dimensionless frequency which is defined in this work as $(\omega * H_1)/C_{\text{S soil layer}}$. Surface amplifications are determined for a suite of dimensionless frequencies (0·5, 1·0, 1·2, 1·4, 1·6, 1·8, 2·0, 2·5, and 3·0). In the case of a soil layer with a shear wave velocity of 1000 fps and a thickness of 20′, these dimensionless frequencies correspond to a frequency range 4·0–23·9 cps.

Besides investigating surface amplifications using a two-dimensional analysis, an objective of this study is to determine the distance from the vertical rock discontinuity in Figure 1 that two-dimensional analysis results are similar to the results of a one-dimensional analysis study. The nearest point on each side of the rock discontinuity where the surface amplification of a two-dimensional analysis is within 10% of the solution of the one-dimensional analysis, is defined in this study to be the scattering limit point. Consequently, this point defines an area range within which surface displacement is affected due to the additional scattering caused by the rock discontinuity. Conversely, surface amplifications outside of this range are not affected by the discontinuity and can therefore be easily calculated using a one-dimensional analysis. Plots of scattering limits for each of the scenarios are provided as a function of the dimensionless frequency.

The two-dimensional investigation was made using a code developed by the author applying the boundary integral equation method in the frequency domain. In the development of the code, the domain boundaries were approximated using linear elements. In formulating a

two-dimensional solution, the boundary integral equation method was selected due to the technique's inherent advantages. These advantages include:

1. in the boundary element method the topography and soil are able to be accurately modelled;
2. the domain problem is simplified to a boundary problem;
3. the radiation condition is automatically satisfied and non-reflecting boundaries are not required.

2. ANTI-PLANE BOUNDARY INTEGRAL EQUATION FORMULATION

The governing equation for the anti-plane two-dimensional analysis is derived from Navier's equation in the time domain which for a linear viscous material is

$$(\lambda + 2\mu)\, u_{j,ji} + \mu (u_{i,jj} - u_{j,ji}) + \eta_p \frac{\partial u_{j,ji}}{\partial t} + \eta_s \frac{\partial (u_{i,jj} - u_{j,ji})}{\partial t} = \rho \ddot{u}_i \tag{1}$$

where u_i is the displacement in the 'i' direction, ρ is the soil density, λ and μ are the Lame' elastic constants, and η_p and η_s are the compression and shear wave viscosity, respectively. The comma in equation (1) represents differentiation. A repeated index in the equation denotes summation. For anti-plane shear wave motion, vector equation (1) simplifies to a scalar equation:

$$\mu (u_{2,jj}) + \eta_s \frac{\partial (u_{2,jj})}{\partial t} = \rho \ddot{u}_2 \tag{2}$$

The boundary integral equation for anti-plane motion is formulated in the frequency domain using a Fourier transform defined as

$$\bar{f}(\omega) = F\{ f(t)\} = \int_0^T f(t)\, \mathrm{e}^{+\mathrm{i}\omega t}\, \mathrm{d}t \tag{3}$$

where ω is angular frequency and t is time. After applying the Fourier transform of equation (3), equation (2) becomes

$$(\mu - \mathrm{i}\omega\eta_s)\, \bar{u}_{2,jj} = -\rho\omega^2\, \bar{u}_2 \tag{4}$$

where the overbar represents the Fourier transform of the variable. Since the input motion is harmonic, a hysteretic damping model is used to convert the linear viscous damping to a hysteretic damping ratio

$$\eta_s = \frac{2\beta_s\, \mu}{\omega} \tag{5}$$

where β_s is the shear wave hysteretic damping. Substituting hysteretic damping for the linear viscous damping, equation (4) becomes

$$\mu^* \bar{u}_{2,jj} = -\rho\omega^2\, \bar{u}_2 \tag{6}$$

where μ^* represents the complex shear modulus which is equal to

$$\mu^* = \mu\, (1 - \mathrm{i}2\beta_s) \tag{7}$$

The boundary integral equation is developed from equation (6). For anti-plane wave motion in a damped material, the boundary integral equation is[14]

$$\bar{u}_2^{\mathrm{i}}(\xi) = \oint_s \left[\bar{u}_2(x, \omega) \frac{\partial u_{22}^*}{\partial n}(x, \xi, \omega) - u_{22}^*(x, \xi, \omega) \frac{\partial \bar{u}_2}{\partial n}(x, \omega) \right] \mathrm{d}S(x) + c(\xi)\, \bar{u}_2(\xi, \omega) \tag{8}$$

where the integral is taken in the Cauchy principal value sense. In equation (8), n is the normal of the boundary surface at x. $u_{22}^*(x, \xi, \omega)$ and $(\partial u_{22}^*/\partial n)(x, \xi, \omega)$ are the displacement and traction influence functions, respectively, for anti-plane motion. $c(\xi)$ is a constant which accounts for the singularity of the traction influence function at ξ. $\bar{u}_2^{\mathrm{i}}(\xi)$ is the incident wave displacement at ξ. For a half-space domain, $\bar{u}_2^{\mathrm{i}}(\xi)$ is equal to

$$(u_2)_{\mathrm{hs}}^{\mathrm{i}}(x, \omega) = (A_{\mathrm{sh}})_{\mathrm{hs}} \exp\{-\mathrm{i}kt_{\mathrm{hs}}\, x_3\} \exp\{+\mathrm{i}kx_1\} \tag{9}$$

where $(A_{\mathrm{sh}})_{\mathrm{hs}}$ is the half-space incident wave magnitude, k is the wave number, and t_{hs} is given as

$$t_{\mathrm{hs}} = \sqrt{\frac{1}{[(m_x)_{\mathrm{hs}}]^2} - 1} \tag{10}$$

where $(m_x)_{\mathrm{hs}}$ is the cosine of the half-space incident wave angle. For regions other than the half-space, the left-hand side of equation (8) is set to zero.

The displacement influence function, u_{22}^*, in equation (8) is the displacement at the field point x due to a unit load at the source point ξ and is equal to:[15]

$$u_{22}^*(x, \xi, \omega) = \frac{\mathrm{i}}{4} H_0^{(1)}(k_{\mathrm{s}}^* r) \tag{11}$$

where $H_0^{(1)}(x)$ is the Hankel function of the first kind of 0 order and r is the distance from the source point, ξ, to the field point x. The full-space displacement influence function is used because of its applicability to multi-domain problems. In equation (11), k_{s}^* is the complex shear wave number which is derived using the complex shear modulus of equation (7):

$$k_{\mathrm{s}}^* = \frac{\omega}{\sqrt{\mu^*/\rho}} \tag{12}$$

The traction influence function, $(\partial u_{22}^*/\partial n)(x, \xi, \omega)$, is the traction at x due to a unit force at ξ in the x_2 direction. It can be derived from equation (11) by differentiating $u_{22}^*(x, \xi, \omega)$ with respect to n at the field point x:

$$\frac{\partial u_{22}^*}{\partial n}(x, \xi, \omega) = -\frac{\mathrm{i}}{4} H_1^{(1)}(k_{\mathrm{s}}^* r) \frac{\partial r}{\partial n} \tag{13}$$

The boundary integral equation (8) is satisfied in each of the homogeneous domains of the problem in Figure 1. In order to solve equation (8), integration is performed by discretizing the boundary surfaces into boundary elements in each of the domains and numerically integrating. Theoretically, each boundary is to be discretized for the entire length of the domain. For enclosed domains, this poses no problem, however, open domains include boundaries which extend to infinity. In these cases, the length of the boundary which can be discretized is limited. For open domains with high damping this does not present a problem. The boundary can be discretized to a point well outside of the study area so that results within the study area are reliable. Conversely,

for cases of low damping, limiting the boundary of an open domain causes inaccurate results. Following, an alternative approach is discussed in order to more accurately model the behaviour of configurations which include open domains.

3. LAYER TRUNCATION CORRECTION

The problem of discretizing an open domain area is shown in Figure 2 for a soil layer with a surface irregularity on a rock half-space. The procedure discussed here for the layer truncation correction is similar to the method proposed by Hadley *et al.*[10] for elastic soil layers. S′ side and S″ side represent fictitious boundaries that are used to make the open soil layer domain closed. These boundaries are located at a distance far enough from any anomaly in the soil configuration so that scattering along these boundaries due to the anomaly is negligible. If this is true, displacements and tractions along the fictitious boundaries can be taken as the solutions from a one-dimensional analysis. Therefore, the boundary integral equation for the soil layer can be written as

$$\bar{u}_2^{\mathrm{i}}(\xi) = \oint_{S_1+S_2} \left[\bar{u}_2(x,\omega)\frac{\partial u_{22}^*}{\partial n}(x,\xi,\omega) - u_{22}^*(x,\xi,\omega)\frac{\partial \bar{u}_2}{\partial n}(x,\omega) \right] \mathrm{d}S(x) + c(\xi)\,\bar{u}_2(\xi,\omega)$$
$$+ \oint_{S' \text{ side}+S'' \text{ side}} \left[\bar{u}_2^{\mathrm{ff}}(x,\omega)\frac{\partial u_{22}^*}{\partial n}(x,\xi,\omega) - u_{22}^*(x,\xi,\omega)\frac{\partial \bar{u}_2^{\mathrm{ff}}}{\partial n}(x,\omega) \right] \mathrm{d}S(x) \qquad (14)$$

where the ff superscript represents values from the one-dimensional solution. A more detailed explanation of the approach is included in Reference 16.

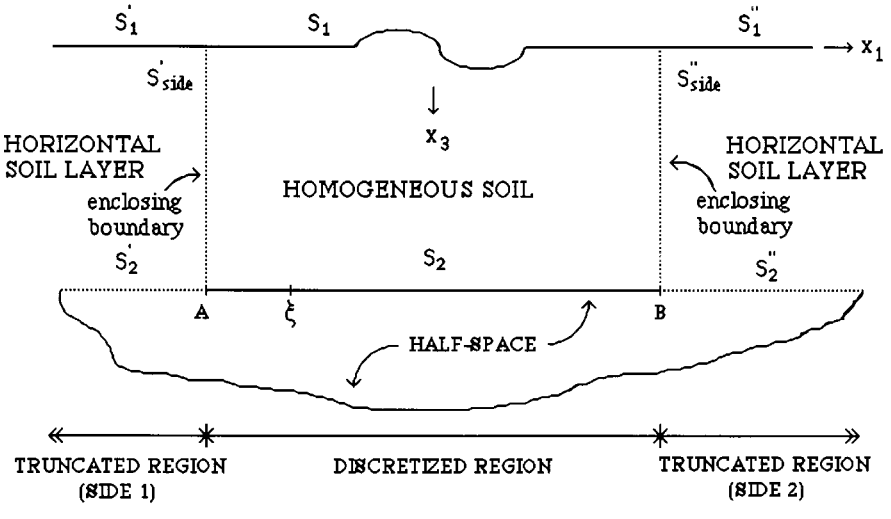

Figure 2. Correction for truncation

4. HALF-SPACE TRUNCATION CORRECTION

The limited range for the discretization of the half-space boundary is shown in Figure 2. In order to include for the effect of the part of the half-space boundary which is not discretized, displacements and tractions outside the discretized region are assumed to have values which correspond to the solutions of a one-dimensional analysis. Consequently, equation (8) can be written for the half-space region as

$$\begin{aligned}\bar{u}_2^{\mathrm{i}}(\xi) = &\int_{+\infty}^{\mathrm{B}} \frac{\mathrm{i}}{4} H_0^{(1)}([k_{\mathrm{s}}]_{\mathrm{hs}}\, r)\, \frac{\partial(\bar{u}_2\,(x_1 = 0, x_3 = H_{\mathrm{hs}}, \omega))_{\text{side 2}}}{\partial x_3} \exp(\mathrm{i}kx_1)\, \mathrm{d}S(x) \\ &+ \int_{\mathrm{A}}^{-\infty} \frac{\mathrm{i}}{4} H_0^{(1)}([k_{\mathrm{s}}]_{\mathrm{hs}}\, r)\, \frac{\partial(\bar{u}_2\,(x_1 = 0, x_3 = H_{\mathrm{hs}}, \omega))_{\text{side 1}}}{\partial x_3} \exp(\mathrm{i}kx_1)\, \mathrm{d}S(x) \\ &- \oint_{\mathrm{B}}^{\mathrm{A}} \frac{\mathrm{i}}{4} H_0^{(1)}([k_{\mathrm{s}}]_{\mathrm{hs}}\, r)\, \frac{\partial \bar{u}_2\,(x, \omega)}{\partial n}\, \mathrm{d}S(x) + c(\xi)\bar{u}_2(\xi)\end{aligned} \tag{15}$$

where H_{hs} is the depth from the surface to the half-space boundary. The first two integral equations in equation (15) represent the half-space correction for truncation which is typically neglected in analyses. Considering the boundary of the half-space region to be horizontal and the half-space material elastic, the half-space truncation correction can be written as

half-space correction for truncation

$$\begin{aligned}= &+\frac{\mathrm{i}}{4}\exp(\mathrm{i}\,[k_{\mathrm{s}}]_{\mathrm{hs}}\,[m_{\mathrm{x}}]_{\mathrm{hs}}\,\xi) \\ &\left[\left[\frac{[(\bar{u}_2)^{\mathrm{ff}}]_{\text{side 1}}}{\partial x_3}\,(x_1 = 0,\, x_3 = H_{\mathrm{hs}},\, \omega)\right]\right. \\ &\times\left\{\frac{1}{[k_{\mathrm{s}}]_{\mathrm{hs}}\,\sqrt{1 - [m_{\mathrm{x}}]_{\mathrm{hs}}^2}}\left(1 + \frac{2(\pi/2 - \theta_{\mathrm{hs}})}{\pi}\right) - \int_{r=0}^{\xi - A} H_0^{(1)}\,([k_{\mathrm{s}}]_{\mathrm{hs}}\, r)\exp(-\mathrm{i}[k_{\mathrm{s}}]_{\mathrm{hs}}\,[m_{\mathrm{x}}]_{\mathrm{hs}}\, r)\, \mathrm{d}r\right\} \\ &+\left[\frac{\partial\,[(\bar{u}_2)^{\mathrm{ff}}]_{\text{side 2}}}{\partial x_3}\,(x_1 = 0,\, x_3 = H_{\mathrm{hs}},\, \omega)\right] \\ &\left.\times\left\{\frac{1}{[k_{\mathrm{s}}]_{\mathrm{hs}}\,\sqrt{1 - [m_{\mathrm{x}}]_{\mathrm{hs}}^2}}\left(1 - \frac{2(\pi/2 - \theta_{\mathrm{hs}})}{\pi}\right) - \int_{r=0}^{\mathrm{B} - \xi} H_0^{(1)}\,([k_{\mathrm{s}}]_{\mathrm{hs}}\, r)\exp(+\mathrm{i}[k_{\mathrm{s}}]_{\mathrm{hs}}\,[m_{\mathrm{x}}]_{\mathrm{hs}} r)\mathrm{d}r\right\}\right]\end{aligned} \tag{16}$$

Development of the method for the correction of half-space truncation is presented in detail in Reference 16. By incorporating equation (16), the entire boundary of the half-space is considered in the two-dimensional analysis.

5. CODE VALIDATION

The boundary element code used in the analysis was developed by the author. Problems with known analytic solutions were compared with results from the code to validate its use. Three problems were investigated. The first test problem compared the analytic solution[10] and the

numerical solution for a cavity with a radius R in an elastic full-space. Results using the boundary element method showed excellent agreement with the analytic solution. The second problem used to test the code was the analytic solution derived by Trifunic[4] for the amplification of an anti-plane wave in a half-space with a semi-circular canyon. Comparison of the analytic solution to the numerical solution was made considering no correction for the truncation of the half-space boundary. Even without this correction, the numerical solution showed good agreement with the analytic solution. For the third test problem, a soil layer on a half-space was investigated. This

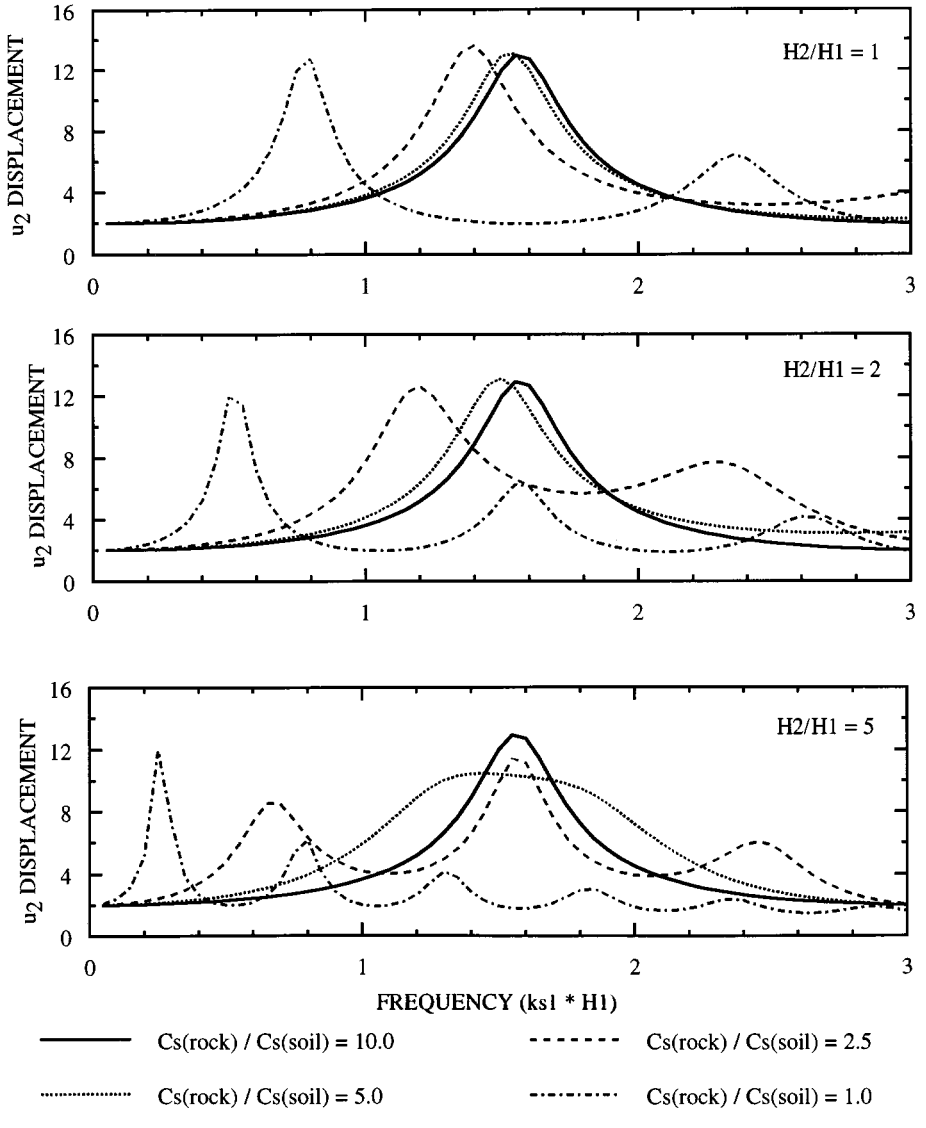

Figure 3. One-dimensional analysis of antiplane surface displacement due to a vertically incident unit SH wave

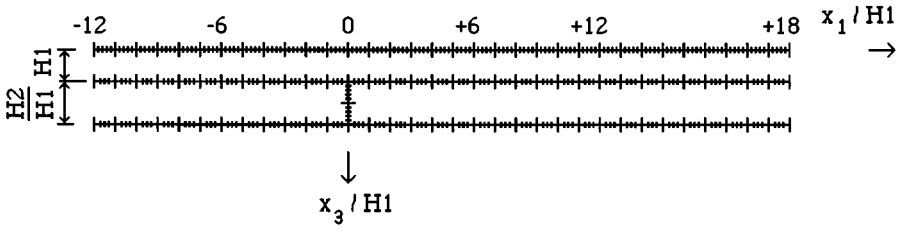

Figure 4. Boundary discretization

Table II. Natural frequencies and corresponding surface amplitudes due to an incident SH wave

Surface displacement

CS2/CS1	H2/H1	1st natural frequency $n = 1$ (fundamental frequency)				2nd natural frequency $n = 2$			
		ks1 * H1	θ incident			ks1 * H1	θ incident		
			90·0	75·0	60·0		90·0	75·0	60·0
1·0	1·0	0·8	12·7	12·5	11·8	2·4	6·4	6·3	6·1
	2·0	0·5	12·0	11·8	11·2	1·6	6·3	6·2	6·0
	5·0	0·3	12·0	11·8	11·2	0·8	6·2	6·1	6·0
2·5	1·0	1·4	13·6	13·3	12·4	3·7	6·4	6·2	5·8
	2·0	1·2	12·6	12·3	11·4	2·3	7·7	7·5	7·0
	5·0	0·7	8·5	8·3	7·6	1·6	11·4	11·2	10·5
5·0	1·0	1·6	13·0	12·8	12·1	4·6	7·2	7·1	6·7
	2·0	1·5	13·1	12·9	12·1	4·8	7·0	6·9	6·5
	5·0	1·5	10·5	10·3	10·0	4·7	6·8	6·7	6·4
10	1·0	1·6	12·9	12·7	12·0	4·7	6·4	6·3	6·1
	2·0	1·6	12·9	12·7	12·0	4·7	6·4	6·3	6·1
	5·0	1·6	12·9	12·7	12·0	4·7	6·4	6·3	6·1

problem was examined in order to demonstrate the significance of the correction for domain truncation. The results between the analytic and boundary element method using the correction for truncation had good agreement. Details including results about the validation of the boundary element code are given in Reference 14.

6. ONE-DIMENSIONAL ANALYSIS

A one-dimensional analysis was performed as a preliminary investigation for the behaviour of the soil configuration in Figure 1 assuming no scattering due to the rock discontinuity. The study used an array of incidence angles: 90, 75, and 60°. Results for a vertically incident unit SH wave

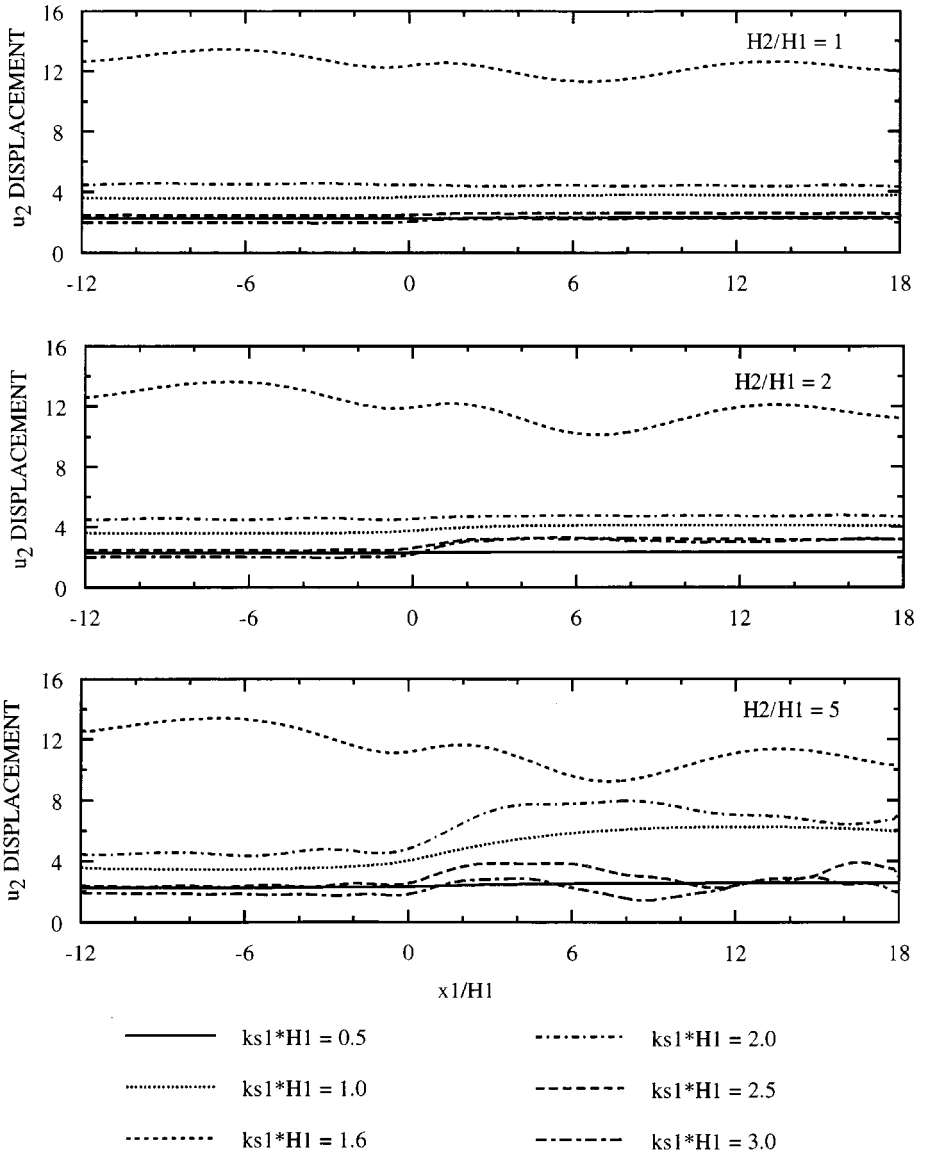

Figure 5. u_2 surface displacement due to a vertical unit incident SH wave, Cs rock "A"/Cs soil = 5

are given in Figure 3. Results for the various incidence angles are summarized in Table I for the first and second natural frequencies of the soil profile. In the study, surface displacements showed small variance for the incidence angles considered.[14] The differences in the results determined using a one-dimensional analysis indicates the degree of interaction that could be expected to occur in the region adjacent to the rock discontinuity. In order to include for this interaction, a two-dimensional analysis is required.

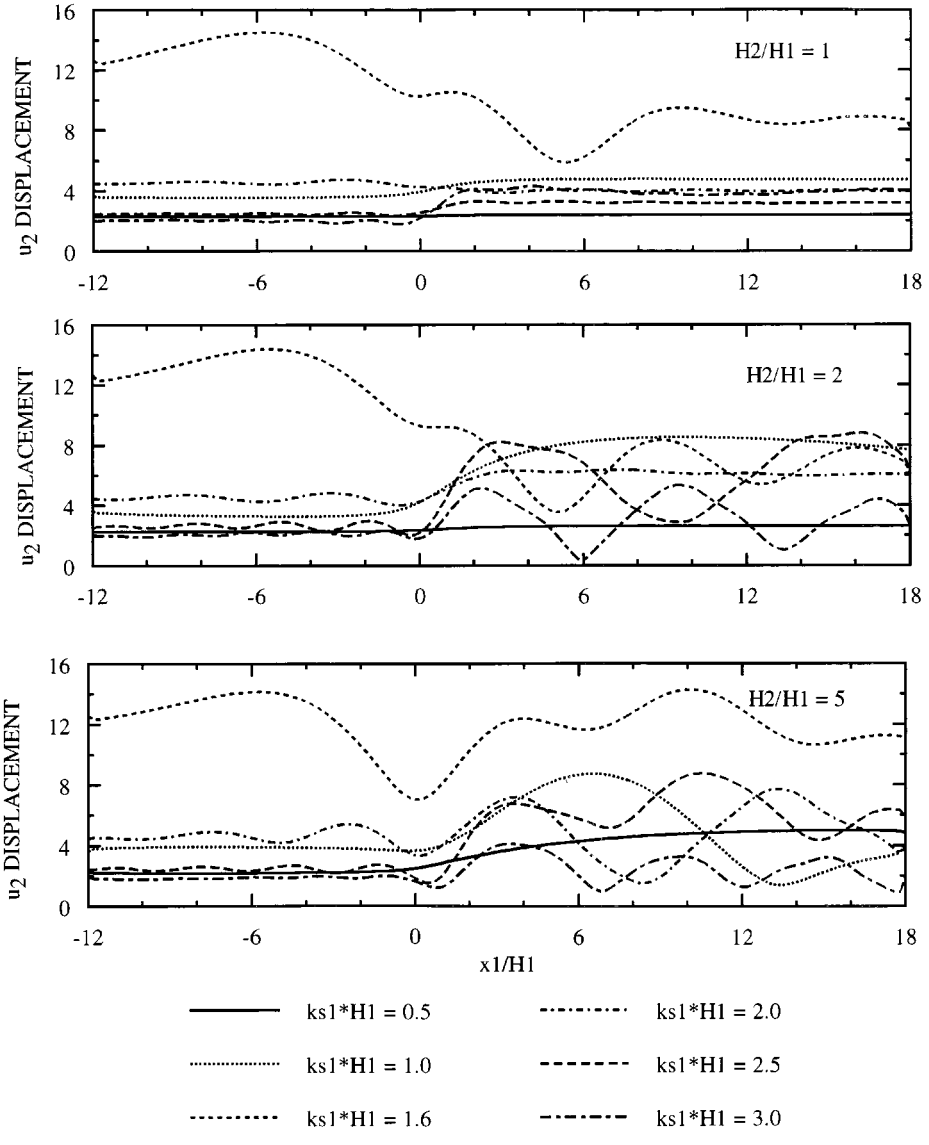

Figure 6. u_2 surface displacement due to a vertical unit incident SH wave, Cs rock "A"/Cs soil = 2·5

7. TWO-DIMENSIONAL ANALYSIS

The boundary element method is used for a two-dimensional study of the soil-bedrock configuration shown in Figure 1. Figure 4 shows the discretization of the soil–rock profile used to investigate the impact of the rock discontinuity. Segment lengths equal to 0·2 * H1 are used along the surface boundary and the vertical boundary between the embedded rock layer and the rock half-space. This segment length corresponds to a length equal to one-tenth the minimum wave

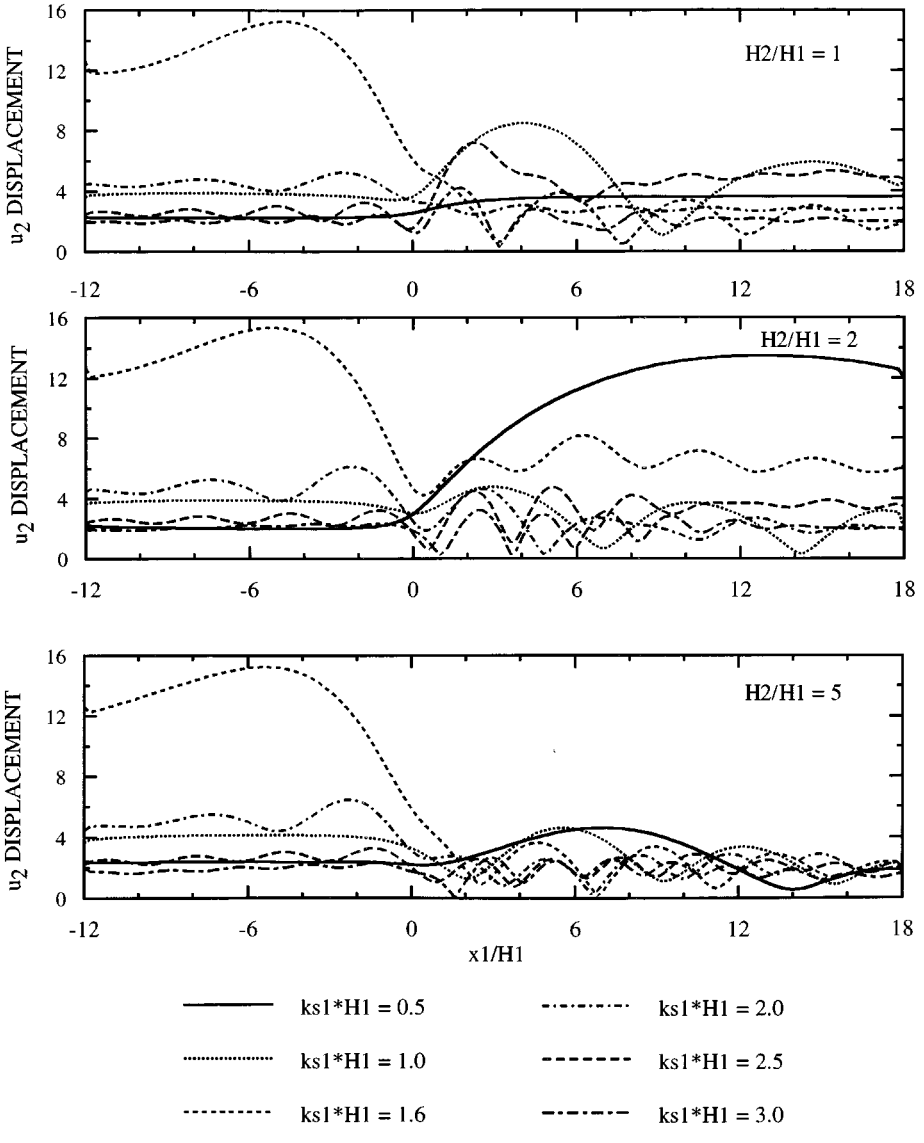

Figure 7. u_2 surface displacement due to a vertical unit incident SH wave, Cs rock "A"/Cs soil = 1

length considered in this study. $0{\cdot}25 * H1$ is used along the other horizontal boundaries. In the region near the intersection point of the three media, the segment length is further reduced to include for the high sensitivity in this local area.

Surface amplifications for a vertically incident unit antiplane shear wave are calculated at dimensionless frequencies, $ks1 * H1$, equal to: 0·5, 1·0, 1·2, 1·4, 1·6, 1·8, 2·0, 2·5, and 3·0, as a function of the thickness ratio and shear wave velocity ratio. Results are given in Figures 5–7 for $ks1 * H1 = 0{\cdot}5$, 1·0, 1·6, 2·0, 2·5, and 3·0 for a vertically incident unit shear wave.

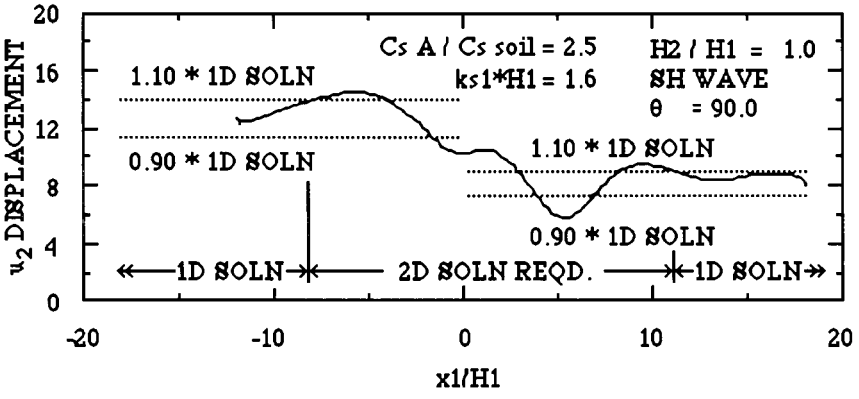

Figure 8. Description of scattering limit distances

Three thickness ratios of the embedded rock are examined: H2/H1 = 1·0, 2·0, and 5·0. Results for the case of the shear wave velocity ratio of the embedded rock to soil equal to 5 are shown in Figure 5. Similarly, Figure 6 includes results for the case of the embedded rock shear velocity ratio equal to 2·5. Lastly, Figure 7 includes the surface amplification plots for when the embedded material is the same as the soil layer, or shear wave velocity ratio equal to 1. The figures are ordered according to increasing effect of the bedrock discontinuity. The figures illustrate that as the differences in the shear stiffness of the embedded rock to half-space increases, the impact of the discontinuity increases. Reviewing the one-dimensional analysis plots in Figure 3, there must exist a transition between the one-dimensional analysis response between $x1/H1 < 0$ and $x1/H1 > 0$ for the various scenarios. Shear waves with higher frequency exhibit greater fluctuation in the discontinuity vicinity, $x1/H1 = 0$. From the two-dimensional analysis figures it is difficult to conclude the impact of the height of the embedded rock layer. From scattering limit curves, discussed later in the paper, the transition zone increases as the thickness of the embedded layer increases. In order to include for the previously discussed correction for truncation, solutions at the end of the discretized zones, $x1/H1 = -12$ and $x1/H1 = +18$, are assumed equal to the one-dimensional solution. Results considering incidence angles of 75 and 60° showed little variation in surface amplification as compared to the curves presented in Figures 5–7.[14]

8. SCATTERING LIMITS

Solutions from the one-dimensional and the two-dimensional analyses are compared by determining at what distance from the origin, $x1/H1 = 0·0$, that the two solutions are similar. These points, which will be referred to here as scattering limit points, indicate areas outside of which a one-dimensional solution suffices. The procedure in developing these locations is shown in Figure 8. The scattering limit points are determined by finding the location outside of which surface displacement for the two-dimensional analysis deviates less than 10% from the one-dimensional solution. In cases where there is reduction of the motion, surface amplifications less than 1·0, the maximum permissible variance from the one-dimensional solution for determining the scattering limit point is taken as $\pm 0·1$. Plots of scattering limits as a function of shear wave

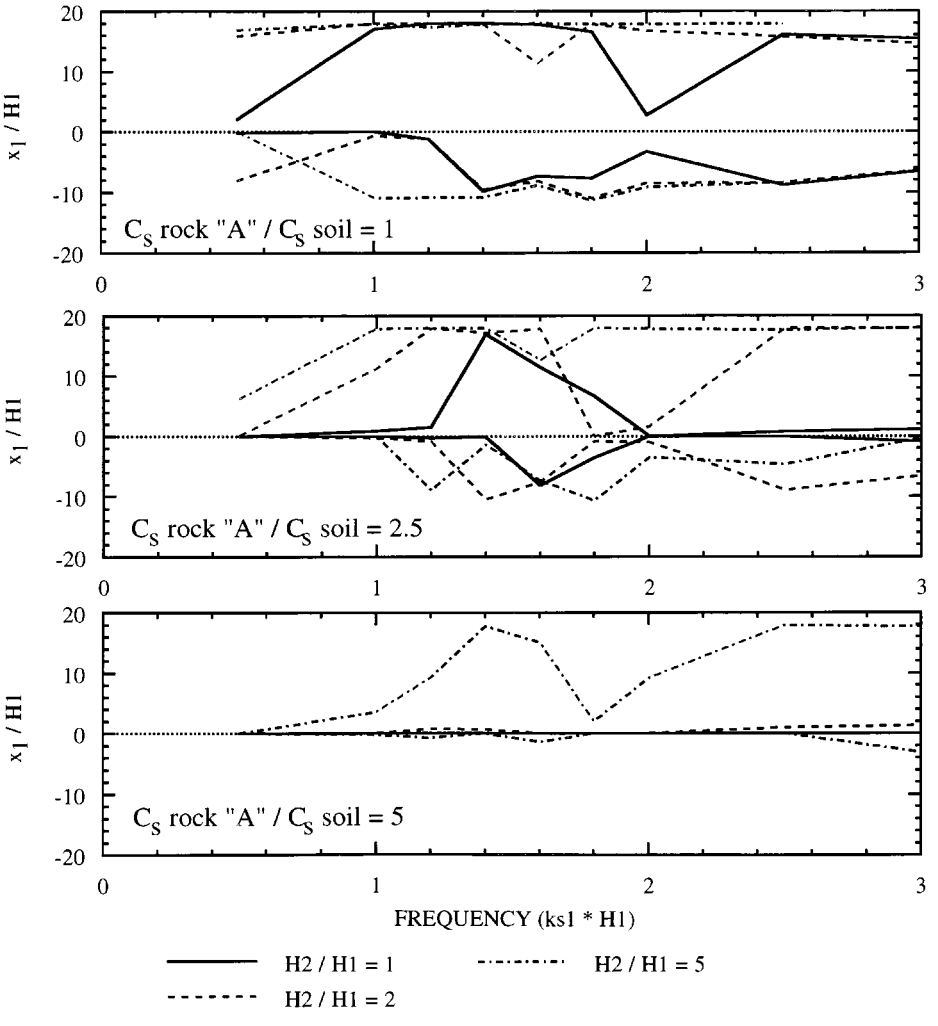

Figure 9. u_2 scattering limits due to a vertical unit incident SH wave

velocity ratio and thickness ratio in the two-dimensional study are given in Figure 9. The figures indicate the location of the scattering limit points in terms of x1/H1 on each side of the origin as a function of the dimensionless frequency, ks1 * H1. Since the end points are forced to equal the one-dimensional solution, maximum values are limited to the bounds of the discretized boundary. Therefore, scattering limits in these figures are restricted to occur within the range of -12 and $+18$.

Figure 9 indicates that the rock discontinuity has greater impact in the area above the embedded rock layer. Increasing the thickness or decreasing the shear wave velocity of the embedded rock causes an increase in the area in which scattering occurs. Although results are given only for vertical incidence, generally scattering limits increase as the angle of incidence becomes shallower.[14]

9. CONCLUSION

A method has been described in order to determine the distance away from a scattering source that a one-dimensional solution suffices. This distance is determined by comparing the surface amplifications from a two-dimensional analysis and a one-dimensional analysis. The point in which both solutions for the two analyses are similar in magnitude defines the scattering limit point. A study was executed considering a vertically incident shear wave on a particular soil–rock configuration. The configuration includes a soil layer resting on a rock half-space which includes an embedded layer. Surface amplifications along with scattering limits were developed for an array of embedded rock thickness and shear wave velocity ratios. A range of dimensionless frequencies were considered. Results from the study indicate that as the thickness of the embedded rock layer increases or the stiffness of the rock layer decreases, the impact of the rock discontinuity on surface amplification increases.

REFERENCES

1. F. J. Sanchez-Sesma, 'Site effects on strong ground motion', *Soil Dyn. Earthquake Engng.* **6**, 124–132 (1987).
2. J. M. Roesset, *Fundamentals of Soil Amplification*, Department of Civil Engineering, Massachusetts Institute of Technology, March 1969.
3. J. P. Wolf, *Dynamic Soil-Structure Interaction*, Prentice-Hall, Inc., Englewood Cliffs, NJ, 1985, pp. 114–165.
4. M. D. Trifunac, 'Surface motion of a semi-cyclindrical Alluvial Valley for incident plane SH waves', *Bull. Seism. Soc. Am.* **61**, 1755–1770 (1971).
5. H. L. Wong and M. D. Trifunac, 'Surface motion of a semielliptical Alluvial Valley for incident plane SH waves', *Bull. Seism. Soc. Am.* **64**, 1389–1408 (1974).
6. M. Dravinski, 'Scattering of SH waves by subsurface topography', *J. Engng. Mech. Div.*, ASCE **108** (EM1), 1–17 (1982).
7. H. Eshraghi and M. Dravinski, 'Transient scattering of elastic waves by dipping layers of arbitrary shape. Part 1: Antiplane strain model', *Earthquake Engng. Struct. Dyn.* **18**, 397–415 (1989).
8. J. Dominguez and R. Abascal, 'Seismic response of strip footings on zoned viscoelastic soils', *J. Engng. Mech.* **115** (5), 913–934 (1989).
9. R. F. Vogt, J. P. Wolf and H. Bachmann, 'Wave scattering by a canyon of arbitrary shape in a layered half-space', *Earthquakle Engng. Struct. Dyn.* **16**, 803–812 (1988).
10. P. K. Hadley, A. Askar and A. S. Cakmak, 'Scattering of waves by inclusions in a nonhomogeneous elastic half-space solved by boundary element methods', *Technical Report NCEER-89-0027*, National Center for Earthquake Engineering Research, June 15, 1989.
11. M. Bouchon, M. Campillo and S. Gaffet, 'A boundary integral equation-discrete wavenumber representation method to study wave propagation in multilayered media having irregular interfaces', *Bull. Seism. Soc. Am.* **54**, 1134–1140 (1989).
12. M. Bouchon and O. Coutant, 'Calculation of synthetic seismograms in a laterally varying medium by the boundary element – discrete wavenumber method', *Bull. Seism. Soc. Am.* **84**, 1869–1881 (1994).
13. I. M. Idriss and H. B. Seed, 'Seismic response of horizontal soil layers', *J. Soil Mech. Found. Div.* **94** (SM4), 1003–1031 (1968).
14. E. Heymsfield, 'Application of the boundary integral equation method to a discontinuity in bedrock', Ph.D. Thesis, City University of New York, 1995.
15. F. B. Hildebrand, '*Advanced Calculus for Applications*', Prentice-Hall, Inc., Englewood Cliffs, NJ, 1976.
16. E. Heymsfield, 'Infinite domain correction for anti-plane shear waves in a two-dimensional boundary element analysis', *Int. J. Numer. Methods Engng.* **40**, 953–964 (1997).

